



Stability and reusability of amine-functionalized magnetic-cored dendrimer for heavy metal adsorption

Kyung-Joo Kim¹ and Jae-Woo Park^{1,*}

¹Department of Civil and Environmental Engineering, Hanyang University, 222 Wangsimni-ro, Seongdong-gu, Seoul 133-791, South Korea

Received: 13 June 2016

Accepted: 6 September 2016

Published online:

12 September 2016

© Springer Science+Business Media New York 2016

ABSTRACT

The optimal storage period/condition and the number of repeated use with regenerations were studied in this research in order to fully utilize magnetic-cored dendrimers (MDs) terminalized with amine groups as adsorbents. MDs terminalized with amine groups were synthesized and characterized with X ray diffraction, scanning electron microscopy, Fourier transform infrared spectroscopy, thermo-gravimetric analysis, surface area analysis, vibrating sample magnetometry, and zeta potential analysis to confirm successful synthesis. The order of adsorption affinity to the MDs was $Pb^{2+} > Cd^{2+}$. The effective period of the synthesized MDs was 56 days, and the storage condition for the MDs was in a dry vial. Hydrochloric acid was chosen as the desorption agent to evaluate the regeneration efficiency. After seven regeneration cycles, the adsorption efficiency was approximately 80 %, but it gradually decreased to 55 % after fifteen cycles due to insufficient desorption of loaded heavy metal and loss of adsorbent in the acidic condition during the desorption process. Iron leaching from the MD cores and deterioration of organic branches during desorption were the main reasons for the adsorbent loss. The fraction of iron leaching was dependent on the acidity while the organic carbon leaching fraction was not severely affected by the different hydrochloric acid concentrations.

Introduction

Dendrimers exhibit an extensive range of potential applications due to their extraordinary and adjustable physicochemical properties [1, 2]. Attaching functional groups, such as amine, carboxyl, and hydroxyl, as terminal groups of the dendrimers can result in a substantial increase in binding capacity to a variety of ions [3, 4]. These specific characteristics

make dendrimers promising candidates as efficient adsorbents [5, 6]. Golikand et al. [7] synthesized triazine-based dendrimers with a poly(ethylene glycol) core to sorb Cu(II), Ni(II), and Zn(II). Anbia and Haqshenas [8] reported Pb(II) and Cu(II) adsorption to mesoporous carbon nitride functionalized with melamine-based dendrimer amine. Zhao et al. [9] synthesized polyamidoamine (PAMAM)-grafted cellulose nanofibril aerogels for Cr(VI) removal. Xu and

Address correspondence to E-mail: jaewoopark@hanyang.ac.kr

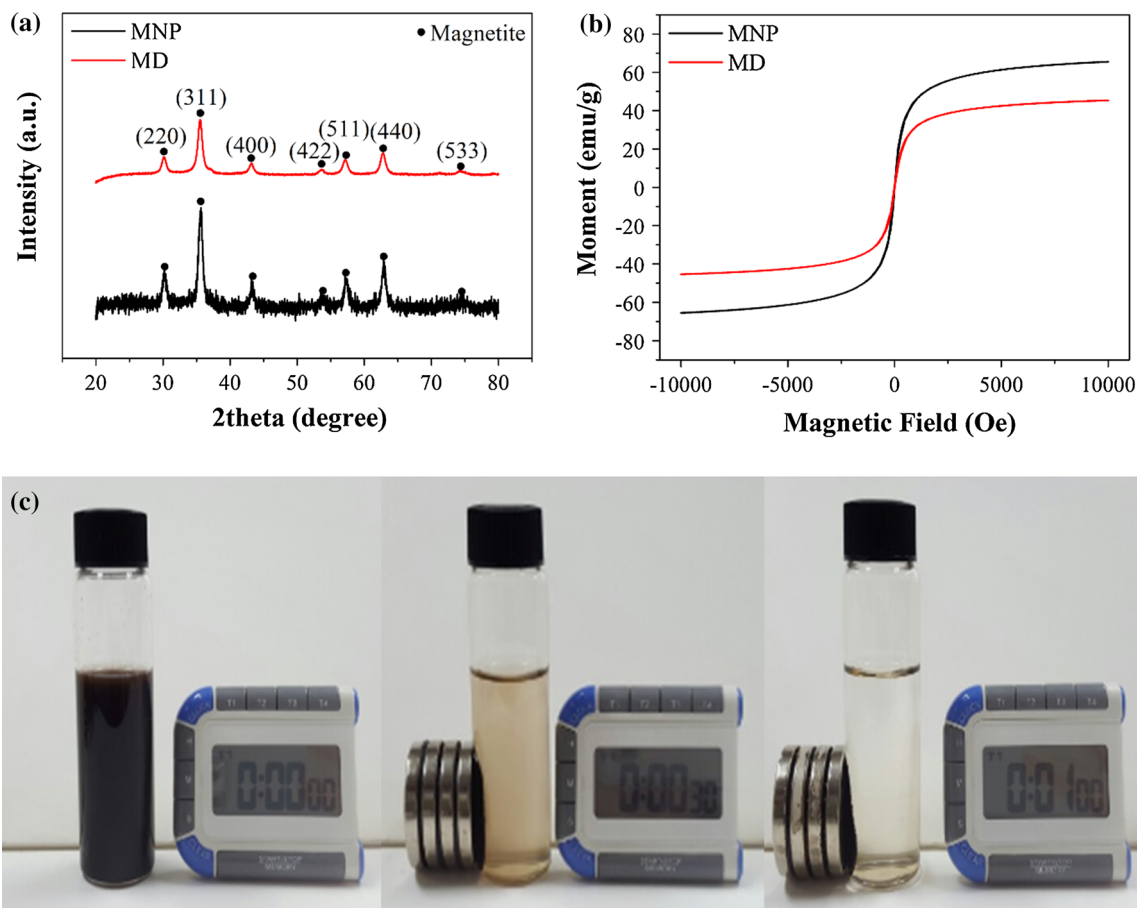


Figure 1 **a** XRD patterns of MNP and MD, **b** magnetization curves of MNP and MD, and **c** MD dispersed in an aqueous solution and magnetic separation.

Zhao [10] investigated PAMAM dendrimers of various generations and terminal functional groups for copper(II) binding. Diallo et al. [11] reported Cu(II) binding to PAMAM dendrimers with terminal amine groups. Cu(II) binding capacities of the PAMAM dendrimers were much greater than those of linear polymers with amine groups. However, separation from the liquid phase is difficult, and filtration, centrifugation, or gravitational separation is required.

Magnetic separation overcomes several limitations of filtration, centrifugation, and gravitational separation [12–16]. Magnetic nanoparticles (MNPs) can be modified using functionalized natural polymers or anthropogenic polymers to enhance surface reactivity for various applications. Dendrimer or polymer structures can be combined with MNPs to achieve facile magnetic separation and high adsorption [17]. Chou and Lien synthesized dendrimer-conjugated MNPs by combining dendrimers with MNPs for

effective removal and recovery of Zn(II) from aqueous solutions [18]. Kim et al. reported magnetite-cored dendrimers (MDs) with TiO₂ terminal groups for significant improvement in methyl orange decolorization [19]. The reusability of spent adsorbents is an important issue in practical applications [20, 21]. MDs as adsorbents can be regenerated by desorbing the ions bound to the terminals groups with acid treatment. However, the stability of the adsorbents can be hampered in repeated regeneration due to component loss and degradation under acidic conditions [22]. Especially in MDs, ferrous ions leached from the magnetic core can stimulate the production of reactive oxygen species that lead to a Fenton reaction and trigger cytotoxicity [23]. Wang and Lo synthesized mesoporous magnetic iron-oxide (γ -Fe₂O₃) as a Cr(VI) adsorbent and monitored the decreased Cr(VI) adsorption in five consecutive regenerations [12]. Singh et al. synthesized amine-

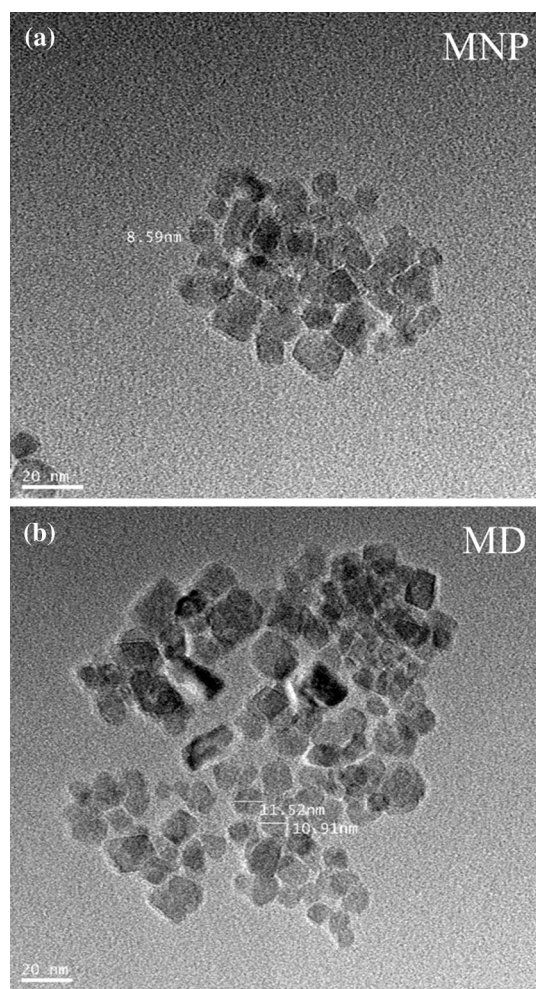


Figure 2 TEM images of **a** MNP and **b** MD.

functionalized Fe_3O_4 and performed repeated adsorption–desorption experiments [24], with the adsorption of Cr(III), Co(II), Ni(II), Cu(II), Cd(II), Pb(II), and As(III) gradually decreasing. Shahbazi et al. [25] synthesized functionalized SBA-15 mesoporous silica by melamine-based dendrimer amines and regenerated the adsorbent for the adsorption of Pb(II), Cu(II), and Cd(II). After four successive regeneration cycles, the adsorption decreased by 4.7 % for Pb(II), 6.3 % for Cu(II), and 5.7 % for Cd(II). Previous researches focused mainly on the experimental observation of adsorption efficiency during repeated regeneration cycles rather than the fundamental cause of the declined adsorption efficiency. Few tried to monitor the stability of the MDs in repeated adsorption–desorption cycles, and this needs to be done to determine the reasons for the declined adsorption.

MDs terminalized with amine groups were synthesized and characterized as efficient adsorbents that could be magnetically separated and recycled for reuse. The objectives of this research were to: (1) investigate the adsorption and desorption of heavy metal ions on synthesized MDs, (2) identify the effective period and optimal storage condition for the synthesized MDs, (3) evaluate the reusability of MDs in repeated adsorption–desorption processes, and (4) identify the deteriorated parts of MDs in the regeneration process.

Materials and methods

Materials

Ferrous sulfate heptahydrate ($\text{FeSO}_4 \cdot 7\text{H}_2\text{O}$), 3-aminopropyltrimethoxysilane (APT, $\text{H}_2\text{N}(\text{CH}_2)_3\text{Si}(\text{OCH}_3)_3$), ethylenediamine (EDA, $\text{NH}_2\text{CH}_2\text{CH}_2\text{NH}_2$), hydrochloric acid (HCl), methanol (CH_4O), lead nitrate ($\text{Pb}(\text{NO}_3)_2$), and cadmium nitrate tetrahydrate ($\text{Cd}(\text{NO}_3)_2 \cdot 4\text{H}_2\text{O}$) were obtained from Sigma-Aldrich (USA). Ferric chloride hexahydrate ($\text{FeCl}_3 \cdot 6\text{H}_2\text{O}$) and methyl acrylate ($\text{CH}_2\text{CHCOOCH}_3$) were purchased from Junsei (Japan). Ammonium hydroxide ($\text{NH}_3 \cdot \text{H}_2\text{O}$) was purchased from Daejung Chemical (Korea). All reagents were used as received without further purification.

MD synthesis

The MNPs in this research were synthesized by coprecipitation of Fe^{2+} and Fe^{3+} ($\text{Fe}^{3+}/\text{Fe}^{2+}$ ratio = 2:1) in the presence of an ammonia solution and treated under hydrothermal conditions [18, 26]. A Fe^{2+} and Fe^{3+} mixture solution was made by dissolving 2.7 g $\text{FeSO}_4 \cdot 7\text{H}_2\text{O}$ and 5.7 g $\text{FeCl}_3 \cdot 6\text{H}_2\text{O}$ into 100 mL of deionized (DI) water. Chemical precipitation was achieved by the addition of NH_4OH solution dropwise to reach pH 10 at 25 °C under vigorous stirring with nitrogen gas purging through the solution during the reaction in order to avoid oxidation of MNPs. The black precipitates were heated at 80 °C for 30 min. The products were washed with DI water and methanol after the reaction.

Two grams of the synthesized MNPs was suspended in 200 mL of methanol. Then, 11.6 mL of APTs was added in drop and the mixture was stirred for 7 h at 60 °C. The products were washed with

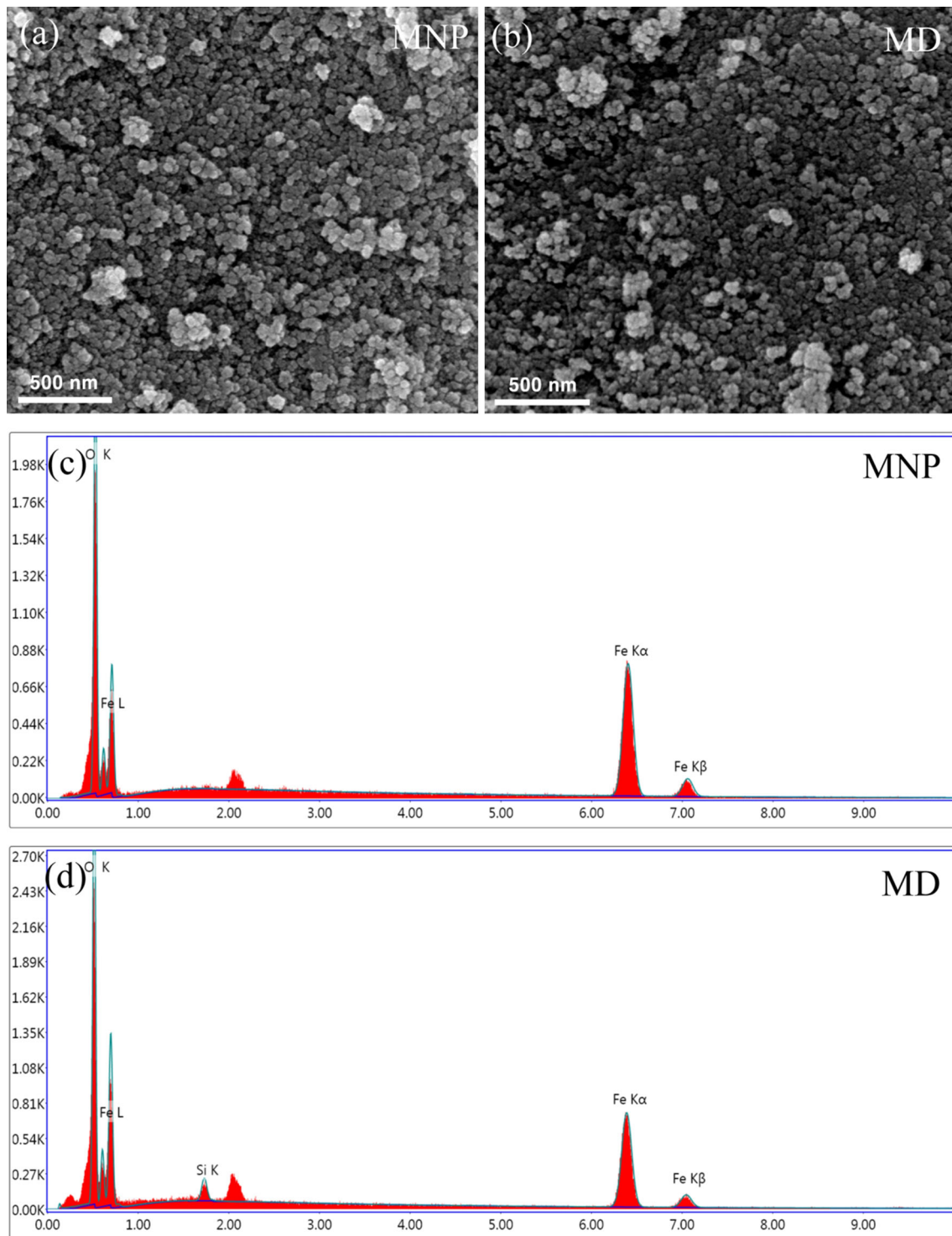


Figure 3 SEM images of **a** MNP, **b** MD, and EDS spectra of **c** MNP, **d** MD.

methanol several times using magnetic separation. In this research, the synthesized MNPs modified only with APT were identified as Generation 0 dendrimer (G0). Two grams of G0 was dispersed in 100 mL of methanol. Then, 20 mL of methyl acrylate was added

in drop. The suspension was ultra-sonicated and stirred at room temperature for 7 h. The products were washed with methanol several times using magnetic separation and then dispersed in 20 mL of methanol. The suspension was stirred at room

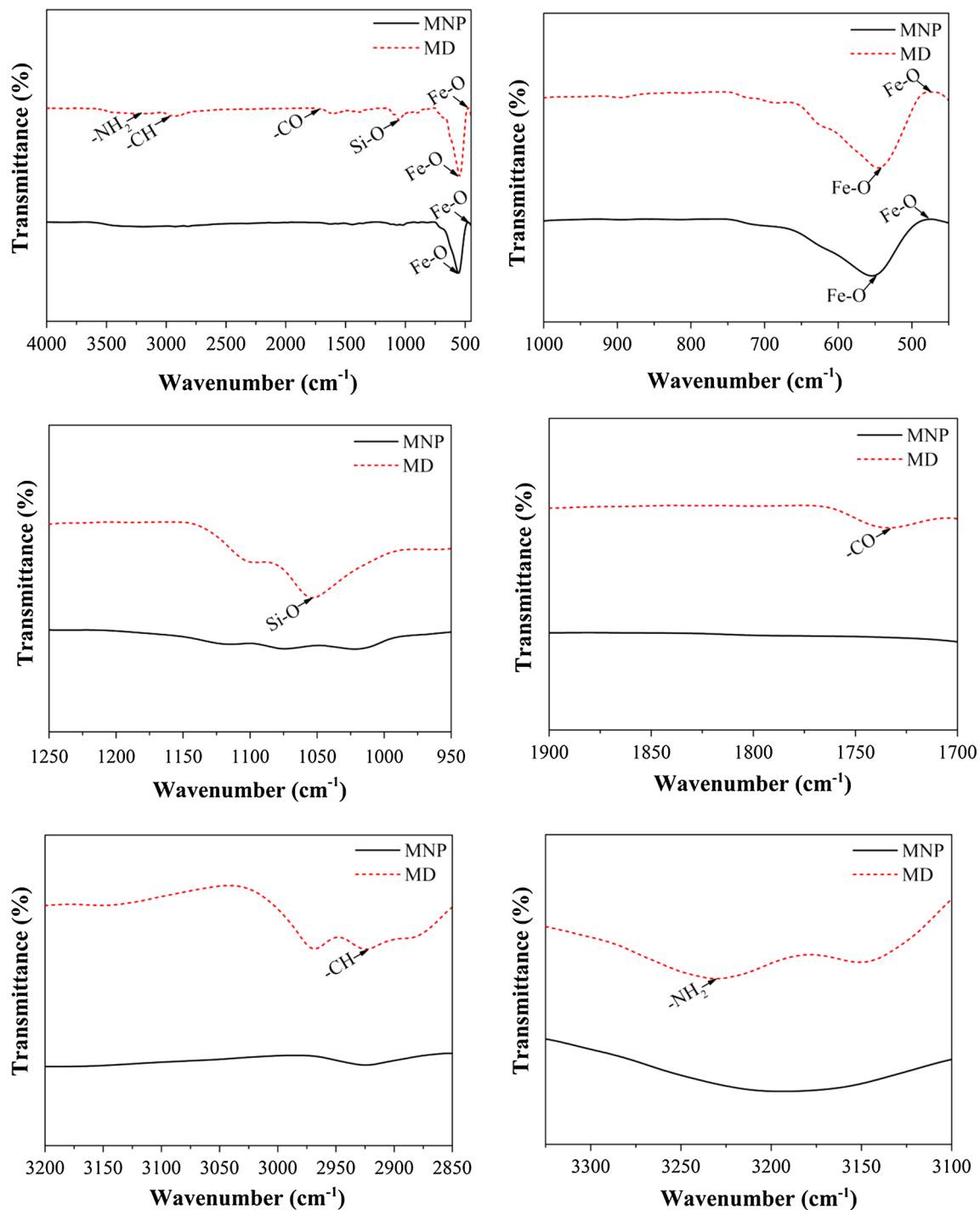


Figure 4 FT-IR spectra of MNP/MD.

temperature for 3 h after 4 mL of EDA was added. After washing with methanol, the solid product was magnetically separated and the supernatant was decanted. The product was dried at 65 °C under vacuum.

Characterization

X-ray diffraction (XRD) patterns were obtained using a Ni-filtered $\text{CuK}\alpha$ source ($\lambda = 1.5418740 \text{ \AA}$, 40 kV, 100 mA) in the range of $2\theta = 20^\circ\text{--}80^\circ$ (D/MAX RINT

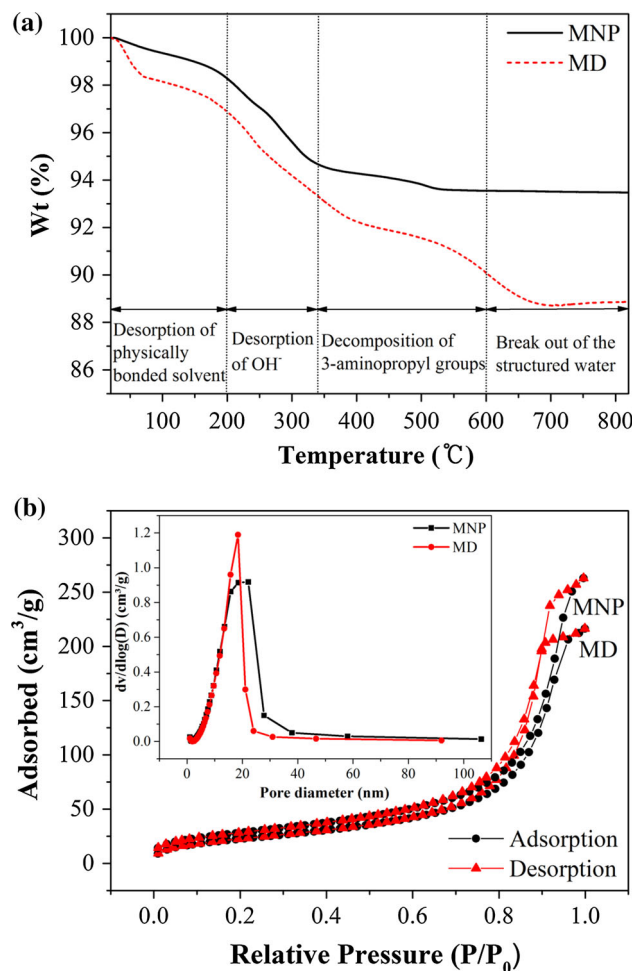


Figure 5 TGA results of **a** MNP/MD, N_2 adsorption–desorption isotherms and pore size distributions (*inset*) of **b** MNP/MD.

2000, Rigaku). Magnetization curves were obtained from a vibrating sample magnetometer (VSM, Quantum Design, PPMS-14). The Fourier transform infrared (FT-IR) spectra were also recorded (UATR Two, PerkinElmer). Thermo-gravimetric analysis (TGA) measurements were performed under a nitrogen atmosphere from 25 to 800 °C at a heating rate of 5 °C/min (SDT Q600, TA Instruments). The specific surface area was analyzed with the Brunauer–Emmett–Teller (BET) model using N_2 adsorption at -196 °C (3 Flex analyzer, Micromeritics). The pore size distribution was derived from the desorption isotherms on the basis of the Barrett–Joyner–Halenda (BJH) method. The zeta potential was also measured (Zetasizer Nano ZS90, Malvern). The size and morphology of the samples were characterized with a scanning electron microscope (SEM) (Nova

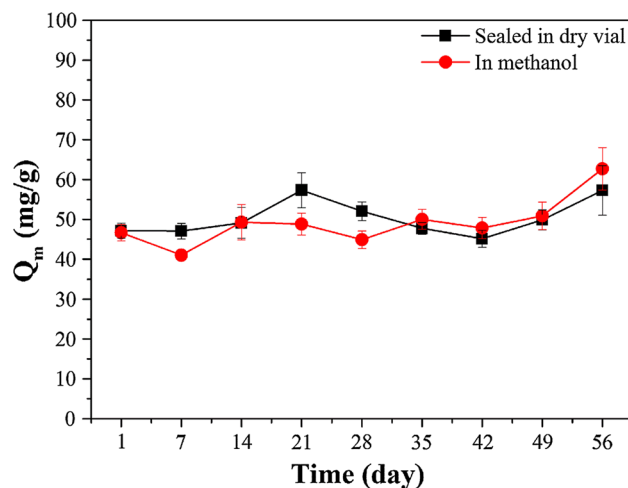


Figure 6 Change in maximal adsorption (Q_m) of lead to MD in two different storage conditions (temperature: 25 °C; contact time: 6 h; lead: 100 mg/L; MD: 0.25 g/L).

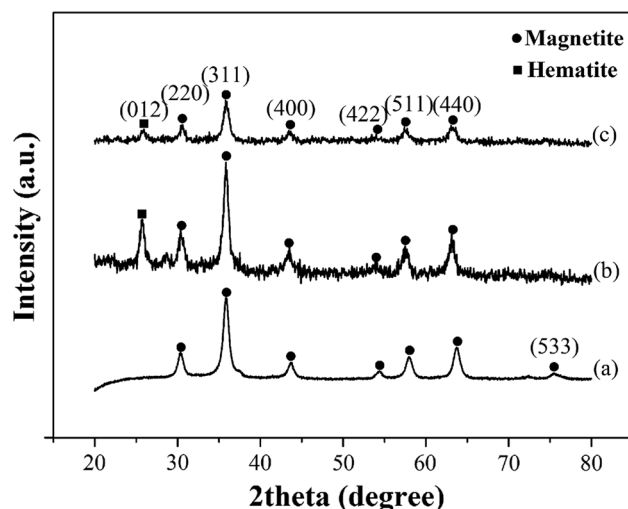
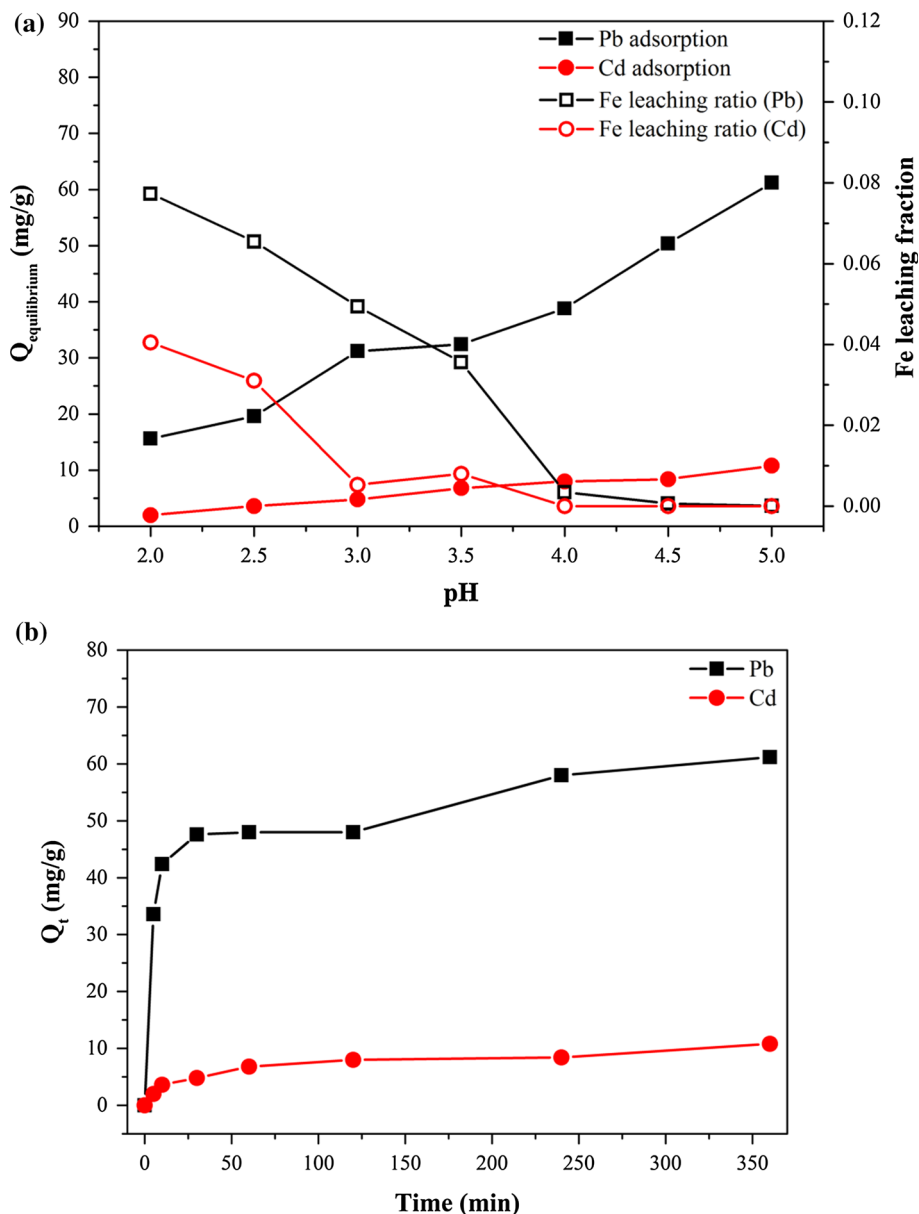


Figure 7 XRD patterns of **a** MD, **b** MD stored in methanol (after 49 days), and **c** MD sealed dry in a vial (after 63 days).

nano SEM 450, FEI) and transmission electron microscope (TEM) (H-8100, Hitachi). Metal ion concentrations in the supernatant were determined with inductively coupled plasma optical emission spectrometry (ICP-OES) (Optima ICP-OES 8000, Perkin Elmer). The detection limits of lead, cadmium, and iron were 2.47, 0.55, and 0.97 $\mu\text{g/L}$, respectively. The organic carbon concentrations in the supernatant were measured with a total organic carbon (TOC) analyzer (TOC-LCPH, Shimadzu). The detection limit of the organic carbon concentration was 4 $\mu\text{g/L}$.

Figure 8 a Effect of pH on the adsorption and Fe leaching fraction of MD (temperature: 25 °C; contact time: 6 h; adsorbate concentration: 100 mg/L; MD: 0.25 g/L), **b** Effect of contact time on the adsorption to the MD (temperature: 25 °C; pH 5.0; adsorbate concentration: 100 mg/L; MD: 0.25 g/L).



Determination of the storage condition and effective period

The produced MDs were stored in methanol or sealed in dry vials to determine a better storage method over an effective storage period. Batch lead adsorption experiments and XRD pattern measurements of the stored MDs were monitored once a week. For adsorption experiments, 10 mg of the MDs was added to a 40 mL lead solution and stirred for 6 h at room temperature. The experiments were performed at an initial pH of 5.0 and the initial lead ion concentration ranged from 10 to 100 mg/L.

Core and organic branch loss

Although low pHs are needed for better regeneration of the used MDs for desorbing adsorbed ions from MDs with proton displacement, organic branches and magnetite cores are also susceptible to decomposition at low pHs [22]. To determine the optimal HCl concentration for regeneration of the used MDs without critical decomposition, 100 mg of the MDs was added to 100 mL of 10^{-4} , 10^{-3} , 1, and 5 M HCl solutions. After continuous stirring for 3, 6, and 24 h, the supernatant was withdrawn to determine HCl concentration for repeated regeneration of MDs. At

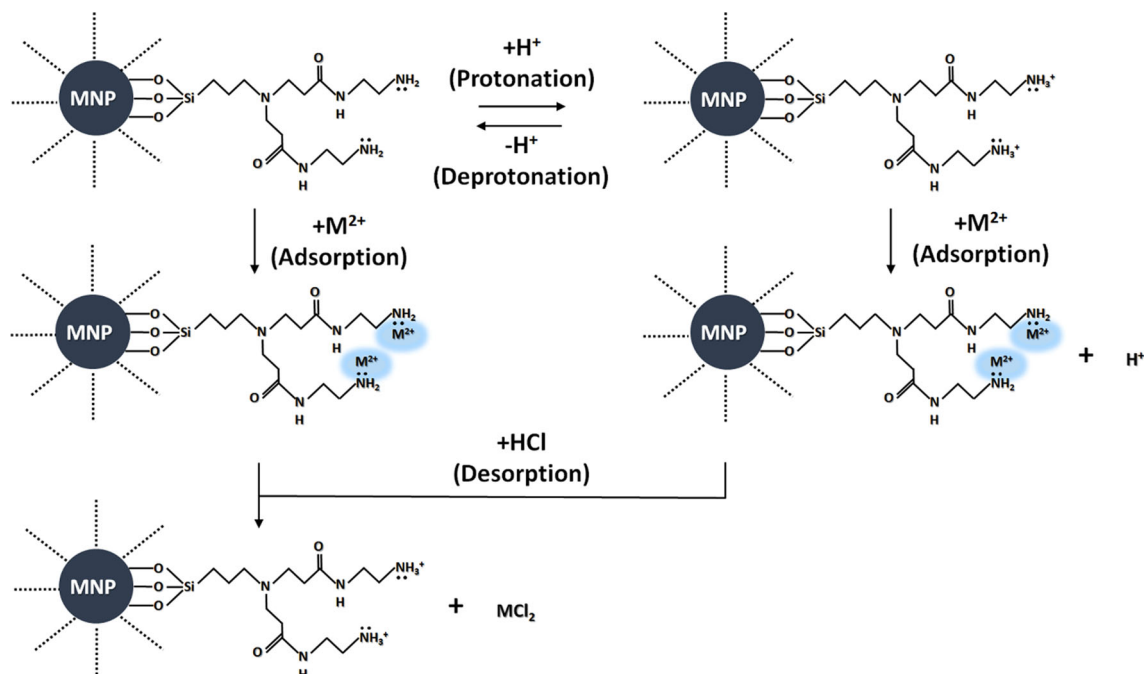


Figure 9 Schematic diagram of metal ion adsorption to MDs in this research.

the determined HCl concentration to the desorption procedure, repeated regeneration experiments were performed. Iron and organic carbon leaching fraction from the MDs were analyzed during loaded metal desorption from the MDs.

MD regeneration

Regeneration of the adsorbent was performed with Cd^{2+} as an adsorbate. The extracting agent in this research was HCl. After 4 h of equilibration, the metal-adsorbed MDs were magnetically separated, added to 40 mL of the extraction solutions, and mixed for 3 h. Subsequently, the MDs were separated with magnetic separation and washed with DI water repeatedly to remove the residual solution for the next adsorption cycle.

Results and discussion

The crystalline structure and magnetic properties were determined via XRD and VSM. Seven typical peaks of magnetite were observed at both MNP and MD in Fig. 1a, confirming that formation of the dendrimer structure has no significant effect on the crystalline characteristics of the nanoparticles. The magnetization curves from the VSM measurement of

MNP and MD with the applied field at 25 °C are presented in Fig. 1b. Hysteresis loops of both MNP and MD indicated typical super-paramagnetic behavior of no hysteresis and an “S” shape [27–29]. The saturation magnetization was 65.50 emu/g and 45.36 emu/g for MNP and MD, respectively. The dendrimer structure formation at MD led to a decrease in the magnetic strength [30, 31]. However, the magnetization of MD was sufficient for separation [32], and MD was efficiently separated within 1 min, as shown in Fig. 1c.

Figure 2 shows the morphology of MNP and MD. Synthesized MNPs have pseudo-cubic structures with length of 8.59 nm. After formation of the dendrimer structure, the average size of MDs was 11.22 nm. An approximately 2.63 nm size increase was observed after the formation of the dendrimer structure, but the shape remained the same, as shown in Figs. 2, 3a, b. The results from the elemental analysis are shown in Fig. 3c, d. The Si K peak was detected due to the APT grafted to the MNP surface after the formation of the dendrimer structure.

Figure 4 shows the FT-IR spectra of MNP and MD. In general, the characteristic bands of magnetite are shown at around 600 and 400 cm^{-1} , which correspond to the Fe–O bond vibration of iron cations at the tetrahedral and octahedral site, respectively [33, 34]. In Fig. 4, the adsorption bands were

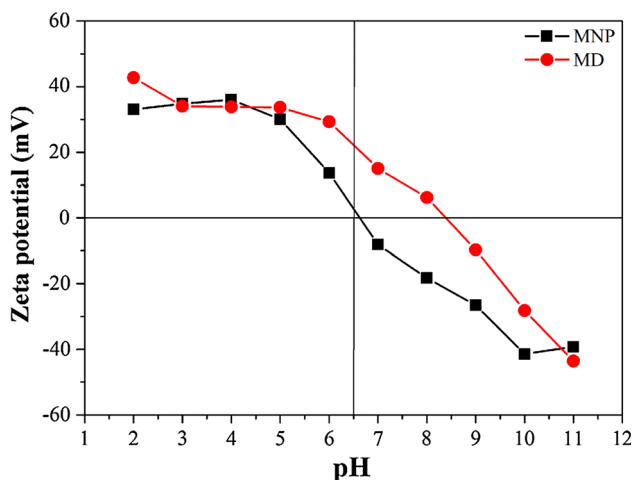


Figure 10 Zeta potential change of MNP and MD as a function of pH.

observed at 548.91 and 472 cm^{-1} for MNP and 545.97 and 488 cm^{-1} for MD, respectively, indicating the formation of magnetite [35–37]. The broad Si–O bands in the range of 900 to 1110 cm^{-1} were observed in MD, confirming the aminosilanization reaction on MNP [19, 38]. The bands assigned to C=O were due to the dendrimer structure at 1733.74 cm^{-1} [19]. In addition, the banding vibrations of –CH (at 2924.27 cm^{-1}) and –NH₂ stretching (at 3230.49 cm^{-1}) are observed in Fig. 4 [39, 40]. Figure 5 shows the TGA results, N₂ adsorption–desorption, and pore size distribution of MNP and MD. TGA analysis of the samples was used to determine the content of the organic branches. The curve was composed of four weight loss steps as shown in Fig. 5a. The first weight loss step below 200 °C can be explained by physically bonded solvent (water and methanol) desorption from the surface [22, 41]. The second weight loss at temperatures ranging from 200 to 340 °C was most likely related to de-hydroxylation (desorption of OH[–]) [42]. The drastic weight loss from 340 to 600 °C corresponds to the thermal decomposition of the 3-aminopropyl groups grafted to the surface. Lastly, the weight loss above 600 °C was associated with the breakout of the structured water [22, 43]. The weight

loss observed at 800 °C was 6.52 and 11.15 % in MNP and MD, respectively. The weight loss in MD was much greater due to the organic branch on the surface of MNP in MD. Figure 5b shows the N₂ adsorption–desorption isotherms and corresponding pore size distributions (inset) calculated with the Barrett–Joyner–Halenda method [44–46]. The specific surface area decreased from 103.23 m^2/g before aminosilanization to 84.14 m^2/g after dendrimer structure generation as the grafted aminosilane groups was anchored to the inner pore volumes [18, 47]. This decrease can be further supported by the decrease in pore size (from 12.97 to 12.04 nm) and pore volume (from 0.41 to 0.33 cm^3/g) after aminosilanization.

No significant difference in maximal adsorption of lead was observed between two different storage conditions, as shown in Fig. 6. However, a new XRD peak corresponding to hematite appeared after some time. The original magnetic core consisted of magnetite, but part of the magnetite was oxidized to hematite, as shown in Fig. 7. Once the core of MDs begins to be oxidized, decrease in recovery rate occurs due to weakened magnetism [48]. The hematite peak was not detected until 56 days when the MDs were sealed in dry vials. Alternatively, the hematite peak was observed after 47 days storage in methanol. Therefore, storage of the synthesized MDs in a dry vial was more suitable than storage in methanol. The effective period of MD was experimentally determined to be 56 days. Thus, all MDs produced in this research were stored in the dry vial condition and used within 56 days.

The effect of pH on the adsorption and Fe leaching fraction of MD is shown in Fig. 8a. Adsorption of Pb and Cd increased with a pH increase from 2.0 to 5.0. This can be explained by competition between H⁺ ions and metal cations. However, at a pH greater than 5.0, metal hydroxide precipitation was observed as Pb(OH)₂ and Cd(OH)₂. To ensure no precipitation, the other adsorption experiments in this research were performed at pH 5.0 [49, 50]. Fe leaching from

Table 1 Kinetics of heavy metal adsorption to MD (temperature: 25 °C; pH 5.0; adsorbate concentration: 100 mg/L; MD: 0.25 g/L)

Metal ions	$q_{e,exp}$ (mg/g)	Pseudo-first-order kinetics			Pseudo-second-order kinetics		
		$q_{e,cal}$ (mg/g)	k_1 (1/min)	R^2	$q_{e,cal}$ (mg/g)	k_2 (g/mg min)	R^2
Pb(II)	61.20	28.75	9.1×10^{-3}	0.78	61.09	1.7×10^{-3}	0.99
Cd(II)	10.80	4.29	9.1×10^{-3}	0.66	10.79	1.2×10^{-2}	0.99

the magnetite core of MDs at different pH is shown in Fig. 8a. The Fe leaching fraction decreased with a pH increase, and negligible Fe leaching was monitored at pH 4.0 and above.

In order to estimate the equilibrium time and to determine the adsorption rate of heavy metals, the effect of contact time on adsorption was studied. The initial metal concentration was 100 mg/L, and the experiments were performed at pH 5 and room temperature under different equilibration times. In Fig. 8b, with an increase in the sorption time from 0 to 30 min, the adsorption of Pb(II) and Cd(II) dramatically rose. After 60 min of contact time, the q_t increased slightly and the plot almost became a straight line after 240 min. Therefore, it is obvious that the equilibrium reached after 360 min of contact time. In order to further analyze the adsorption of heavy metals onto MDs, the kinetics of heavy metal

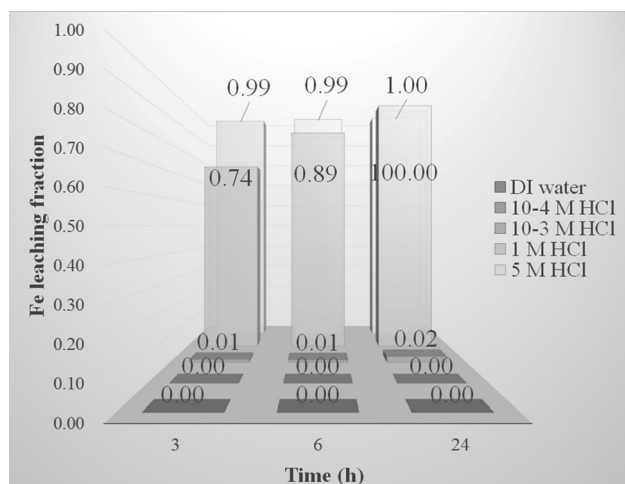


Figure 11 Iron loss from MDs in various desorption periods at different HCl concentrations.

Table 2 Equilibrium model parameters for heavy metal adsorption to MD

Equilibrium model	Single		Binary	
	Pb(II)	Cd(II)	Pb(II)	Cd(II)
Langmuir				
Q_m (mg/g)	170.42	75.17	111.03	67.65
K_L (L/mg)	5.8×10^{-3}	1.4×10^{-3}	1.5×10^{-2}	1.1×10^{-3}
R^2	0.94	0.99	0.92	0.97
Freundlich				
K_F (mg/g)	10.86	0.47	15.84	0.27
n	2.64	1.52	3.58	1.43
R^2	0.98	0.98	0.98	0.95

ions adsorption to the MDs was fitted using pseudo-first-order kinetic and pseudo-second-order kinetic models:

$$\log(q_e - q_t) = \log q_e - \frac{k_1}{2.303} t \quad (1)$$

where q_e and q_t are the adsorbed concentration (mg/g) at equilibrium and at time t (min), respectively, and k_1 is pseudo-first-order rate constant (min^{-1}).

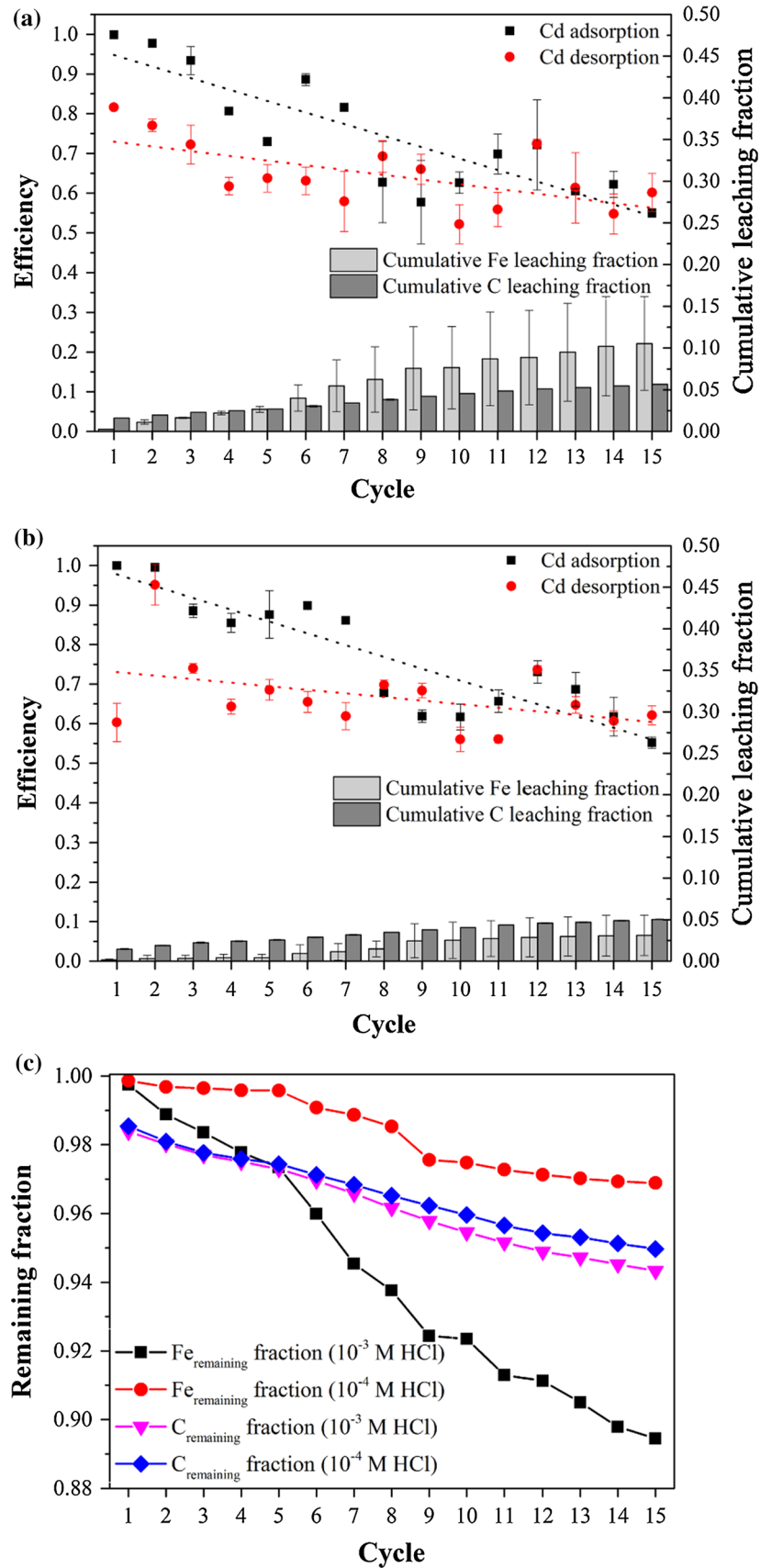
$$\frac{t}{q_t} = \frac{1}{k_2 q_e^2} - \frac{1}{q_e} t, \quad (2)$$

where k_2 is the adsorption rate constant of second order kinetic models.

Table 1 shows the calculated kinetic parameters for lead and cadmium adsorption. The R^2 values of the pseudo-first-order kinetic model for the adsorption of Pb(II) and Cd(II) to the MDs were 0.78 and 0.66, respectively. Those of the pseudo-second-order kinetic model were 0.99 for Pb(II) and 0.99 for Cd(II). In both metal adsorption, q values from the experiments ($q_{e, \text{exp}}$) and calculated from the pseudo-second-order model ($q_{e, \text{cal}}$) was almost identical. It indicates that the pseudo-second-order kinetic model describes the adsorption better than pseudo-first-order kinetic model. The rate-determining step of the adsorption to the MDs is therefore chemical adsorption through valence forces by sharing or switching electrons between the MD and heavy metals [51–54].

Figure 9 shows the schematic diagram of metal ion adsorption to the MDs in this research. Once heavy metal ions (M^{2+}) are reacted with MD, they form coordinate bonds by sharing a lone electron pair of the nitrogen atom in the terminal groups of MDs. Adsorption to the protonated MD is slower than adsorption to non-protonated MD, as the attraction between the nitrogen atom in $-\text{NH}_3^+$ and M^{2+} ions is weaker than the attraction between the nitrogen atom

Figure 12 Regeneration of Cd using **a** 10^{-3} M HCl, **b** 10^{-4} M HCl, **c** and remaining Fe and organic C fraction after regenerations using HCl solutions.



in $-\text{NH}_2$ and M^{2+} ions [55]. Therefore, adsorption to the protonated MD can be regarded as the rate-determining step. Adsorbed heavy metal ions can be desorbed from MDs by reducing the pH using HCl. Figure 10 shows the change of zeta potentials as a function of pH. The zero point charge of the MNPs and MDs in this research was 6.6 and 8.4, respectively. The MNPs and MDs were protonated at $\text{pH} < 6.6$ and $\text{pH} < 8.4$, respectively, and the positive charge density on the surface decreased as the pH increased. Consistent with the pH effect on the adsorption, more NH_2 groups were converted to NH_3^+ at a lower pH. The density of the NH_2 groups on the outer surface of the adsorbent decreases and the adsorption decreases.

Iron loss under various acidic conditions was tested with different desorption equilibration periods to determine the HCl concentration for repeated regeneration of MDs, as shown in Fig. 11. The iron loss was increased with increasing time and HCl concentration. In mild acidic conditions (below 10^{-4} M HCl), iron loss was minimal, irrespective of the equilibration time. Iron loss occurred 10^{-3} M HCl. Seventy-four percent of the iron was lost from MDs after 3 h in 1 M HCl. In 5 M HCl, nearly all of the iron in the MDs leached out. Therefore, 10^{-3} and 10^{-4} M HCl at 3 h were chosen to minimize the MD structure decomposition during desorption.

The results from equilibrium adsorption of Pb(II) and Cd(II) to MDs were fitted to Langmuir and Freundlich models [51, 56, 57].

The Langmuir isotherm model can be expressed as follows:

$$\frac{C_e}{q_e} = \frac{1}{K_L q_m} + \frac{C_e}{q_m} \quad (3)$$

where q_e is the amount of adsorbed metal ions by adsorbent at equilibrium (mg metal/g adsorbent), C_e is the equilibrium metal concentration (mg/L), q_{max} is the maximum metal uptake of the Langmuir isotherm (mg metal/g adsorbent) and K_L (L/mg) is the Langmuir constant which is related to the energy of adsorption.

The Freundlich isotherm model can be presented by the following equation:

$$\log q_e = n \log C_e + \log K_F, \quad (4)$$

where K_F (mg/g) and n are the Freundlich isotherm parameters related to adsorption capacity and adsorption intensity, respectively.

Table 2 shows the model fitting results. The R^2 values for the Langmuir model fitting in single metal system were 0.94 and 0.99 for Pb(II) and Cd(II), respectively. The maximum adsorption of Pb(II) and Cd(II) from the Langmuir fitting in single metal system was 170.42 and 75.17 mg/g, respectively. In binary system, the maximum Pb(II) adsorption from the Langmuir fitting was higher than that of Cd(II) (Pb^{2+} : 111.03 mg/g, Cd^{2+} : 67.65 mg/g). Compared to the single metal system, the maximum adsorption of two metals in binary system decreased due to the competition for the limited adsorption sites in the MDs [58]. The R^2 values for the Langmuir model fitting in binary system were 0.92 and 0.97 for Pb(II) and Cd(II), respectively. The affinity order of adsorption on MD was $\text{Pb(II)} > \text{Cd(II)}$, and this difference arose from the dissimilar chemical properties between the two metals. Lead has a higher Pauling electro-negativity than cadmium (Pb^{2+} : 1.87, Cd^{2+} : 1.69) [59]. Therefore, Pb(II) was subjected more to attraction to the lone electron pairs in donor atoms to form more stable complexes, thus showing higher affinity to the amine functional groups on the surface of the MDs [60]. In addition, Pb(II) has lower $\text{p}K_H$ (negative log of hydrolysis constant) than Cd(II) (Pb^{2+} : 7.71, Cd^{2+} : 10.1), confirming that Pb(II) is more effectively adsorbed through surface complexation or sorption reactions than Cd(II) [61]. Moreover, the different adsorption preferences onto the MDs for Pb(II) and Cd(II) can also be explained by (1) higher atomic weight (Pb^{2+} : 207.2, Cd^{2+} : 112.41) [59], (2) higher ionic radius (Pb^{2+} : 1.21, Cd^{2+} : 0.97) [62], and (3) larger Misono softness value (Pb^{2+} : 3.58, Cd^{2+} : 3.04) [63] of Pb(II).

Figure 12a, b shows the regeneration experimental results of MD for Cd(II) adsorption. After fifteen cycles of adsorption–desorption, the adsorption decreased to 55 % in both cases due to the loss in MD components and insufficient desorption. Compared to the first cycle, the desorption efficiency gradually declined by 17 % at pH 3.0 and 12 % at pH 4.0. During the regeneration process, iron was leached from the magnetic core of MD. More iron was leached from the magnetic core with the stronger acid. After fifteen cycles, the cumulative iron loss fraction was 0.11 with 10^{-3} M HCl and approximately 3.4 times greater than 0.33 with 10^{-4} M HCl. Similar to iron, organic carbon was leached from the organic component of MDs. The cumulative organic carbon loss fraction after fifteen cycles of regeneration was 0.06 with 10^{-3} M HCl and 0.05 with 10^{-4} M HCl.

Figure 12c shows the remaining Fe and organic carbon fraction. The remaining iron content was highly dependent on the acidity while the remaining organic carbon content was not severely affected by the different HCl concentrations.

The higher concentration of HCl resulted in more deterioration of the MD structure, while a nearly negligible difference was observed in the desorption efficiency between 10^{-3} and 10^{-4} M HCl. Therefore, it is better to use a 10^{-4} M HCl solution for 3 h. To achieve better adsorbent reusability, the magnetic core of MDs needs to be more resistant to acidic conditions for enhanced stability and reusability.

Conclusions

In this research, MDs were successfully synthesized for heavy metal adsorption. The effective period of synthesized MDs was 56 days and storage in a dry vial was better than storage in methanol. After seven regeneration cycles, adsorption was maintained at approximately 80 % the original value, but it gradually decreased to 55 % after fifteen cycles. This decrease was caused by insufficient desorption of loaded heavy metal and adsorbent loss due to iron leaching from the MD cores and impairment of organic branches in the acidic condition during the desorption process. More iron loss was observed than organic branch loss during the desorption process. To enhance the stability in repeated MD use as environmental adsorbents, the magnetic core of MDs needs to be more resistant to acidic conditions.

Acknowledgements

This work was supported by Basic Science Research Program through the National Research Foundation of Korea (NRF) funded by the Ministry of Science, ICT & Future Planning (NRF-2015R1A2A1A09005838) and by the Republic of Korea Ministry of Environment as the Green Remediation Research Center for Organic–inorganic Combined Contamination (The GAIA Project-2012000550001).

References

- [1] Satheeshkumar C, Ravivarma M, Rajakumar P, Ashokkumar R, Jeong D-C, Song C (2015) Synthesis, photophysical and

- electrochemical properties of stilbenoid dendrimers with phenothiazine surface group. *Tetrahedron Lett* 56(2):321–326
- [2] Duran-Lara EF, Marple JL, Giesen JA, Fang Y, Jordan JH, Godbey WT et al (2015) Investigation of lysine-functionalized dendrimers as dichlorvos detoxification agents. *Biomacromolecules* 16(11):3434–3444
- [3] Jiang Y, Gao Q, Yu H, Chen Y, Deng F (2007) Intensively competitive adsorption for heavy metal ions by PAMAM-SBA-15 and EDTA-PAMAM-SBA-15 inorganic–organic hybrid materials. *Microporous Mesoporous Mater* 103(1–3):316–324
- [4] Sun C, Qu R, Ji C, Wang C, Sun Y, Yue Z et al (2006) Preparation and adsorption properties of crosslinked polystyrene-supported low-generation diethanolamine-typed dendrimer for metal ions. *Talanta* 70(1):14–19
- [5] Wang Q, Guan Y, Liu X, Ren X, Yang M (2012) High-capacity adsorption of hexavalent chromium from aqueous solution using magnetic microspheres by surface dendrimer graft modification. *J Colloid Interface Sci* 375(1):160–166
- [6] Niu Y, Qu R, Sun C, Wang C, Chen H, Ji C et al (2013) Adsorption of Pb(II) from aqueous solution by silica-gel supported hyperbranched polyamidoamine dendrimers. *J Hazard Mater* 244–245:276–286
- [7] Golikand AN, Didehban K, Irannejad L (2012) Synthesis and characterization of triazine-based dendrimers and their application in metal ion adsorption. *J Appl Polym Sci* 123(2):1245–1251
- [8] Anbia M, Haqshenas M (2015) Adsorption studies of Pb(II) and Cu (II) ions on mesoporous carbon nitride functionalized with melamine-based dendrimer amine. *Int J Environ Sci Technol* 12(8):2649–2664
- [9] Zhao J, Zhang X, He X, Xiao M, Zhang W, Lu C (2015) A super biosorbent from dendrimer poly(amidoamine)-grafted cellulose nanofibril aerogels for effective removal of Cr(vi). *J Mater Chem A* 3(28):14703–14711
- [10] Xu Y, Zhao D (2005) Removal of copper from contaminated soil by use of poly (amidoamine) dendrimers. *Environ Sci Technol* 39(7):2369–2375
- [11] Diallo MS, Christie S, Swaminathan P, Johnson JH, Goddard WA (2005) Dendrimer enhanced ultrafiltration. I. Recovery of Cu (II) from aqueous solutions using PAMAM dendrimers with ethylene diamine core and terminal NH₂ groups. *Environ Sci Technol* 39(5):1366–1377
- [12] Wang P, Lo IM (2009) Synthesis of mesoporous magnetic gamma-Fe₂O₃ and its application to Cr(VI) removal from contaminated water. *Water Res* 43(15):3727–3734
- [13] Badruddoza AZ, Shawon ZB, Tay WJ, Hidajat K, Uddin MS (2013) Fe₃O₄/cyclodextrin polymer nanocomposites for selective heavy metals removal from industrial wastewater. *Carbohydr Polym* 91(1):322–332

- [14] Pang Y, Zeng G, Tang L, Zhang Y, Liu Y, Lei X et al (2011) PEI-grafted magnetic porous powder for highly effective adsorption of heavy metal ions. *Desalination* 281:278–284
- [15] Hao YM, Man C, Hu ZB (2010) Effective removal of Cu(II) ions from aqueous solution by amino-functionalized magnetic nanoparticles. *J Hazard Mater* 184(1–3):392–399
- [16] Vereš J, Orolínová Z (2009) Study of the treated and magnetically modified bentonite as possible sorbents of heavy metals. *Acta Montan Slovaca* 14(2):152–155
- [17] Kainz QM, Reiser O (2014) Polymer-and dendrimer-coated magnetic nanoparticles as versatile supports for catalysts, scavengers, and reagents. *Acc Chem Res* 47(2):667–677
- [18] Chou C-M, Lien H-L (2010) Dendrimer-conjugated magnetic nanoparticles for removal of zinc (II) from aqueous solutions. *J Nanopart Res* 13(5):2099–2107
- [19] Kim L-J, Jang J-W, Park J-W (2014) Nano TiO₂-functionalized magnetic-cored dendrimer as a photocatalyst. *Appl Catal B* 147:973–979
- [20] Banerjee SS, Chen DH (2007) Fast removal of copper ions by gum arabic modified magnetic nano-adsorbent. *J Hazard Mater* 147(3):792–799
- [21] Anirudhan TS, Suchithra PS (2008) Synthesis and characterization of tannin-immobilized hydrotalcite as a potential adsorbent of heavy metal ions in effluent treatments. *Appl Clay Sci* 42(1–2):214–223
- [22] Wang J, Zheng S, Shao Y, Liu J, Xu Z, Zhu D (2010) Amino-functionalized Fe₃O₄@SiO₂ core-shell magnetic nanomaterial as a novel adsorbent for aqueous heavy metals removal. *J Colloid Interface Sci* 349(1):293–299
- [23] Tang SC, Lo IM (2013) Magnetic nanoparticles: essential factors for sustainable environmental applications. *Water Res* 47(8):2613–2632
- [24] Singh S, Barick KC, Bahadur D (2011) Surface engineered magnetic nanoparticles for removal of toxic metal ions and bacterial pathogens. *J Hazard Mater* 192(3):1539–1547
- [25] Shahbazi A, Younesi H, Badieli A (2011) Functionalized SBA-15 mesoporous silica by melamine-based dendrimer amines for adsorptive characteristics of Pb(II), Cu(II) and Cd(II) heavy metal ions in batch and fixed bed column. *Chem Eng J* 168(2):505–518
- [26] Pan B, Cui D, Sheng Y, Ozkan C, Gao F, He R et al (2007) Dendrimer-modified magnetic nanoparticles enhance efficiency of gene delivery system. *Cancer Res* 67(17):8156–8163
- [27] Yan H, Zhang J, You C, Song Z, Yu B, Shen Y (2009) Influences of different synthesis conditions on properties of Fe₃O₄ nanoparticles. *Mater Chem Phys* 113(1):46–52
- [28] Petcharoen K, Sirivat A (2012) Synthesis and characterization of magnetite nanoparticles via the chemical co-precipitation method. *Mater Sci Eng B* 177(5):421–427
- [29] Wu S, Sun A, Zhai F, Wang J, Xu W, Zhang Q et al (2011) Fe₃O₄ magnetic nanoparticles synthesis from tailings by ultrasonic chemical co-precipitation. *Mater Lett* 65(12):1882–1884
- [30] Chandra S, Patel MD, Lang H, Bahadur D (2015) Dendrimer-functionalized magnetic nanoparticles: a new electrode material for electrochemical energy storage devices. *J Power Sources* 280:217–226
- [31] Wang T, Yang W-L, Hong Y, Hou Y-L (2016) Magnetic nanoparticles grafted with amino-riched dendrimer as magnetic flocculant for efficient harvesting of oleaginous microalgae. *Chem Eng J* 297:304–314
- [32] Tavallali H, Deilamy-Rad G, Peykarimah P (2013) Preconcentration and speciation of Cr(III) and Cr(VI) in water and soil samples by spectrometric detection via use of nanosized alumina-coated magnetite solid phase. *Environ Monit Assess* 185(9):7723–7738
- [33] Yu BY, Kwak S-Y (2010) Assembly of magnetite nanocrystals into spherical mesoporous aggregates with a 3-D wormhole-like pore structure. *J Mater Chem* 20(38):8320
- [34] Shebanova ON, Lazor P (2003) Raman spectroscopic study of magnetite (FeFe₂O₄): a new assignment for the vibrational spectrum. *J Solid State Chem* 174(2):424–430
- [35] Kim HR, Jang JW, Park JW (2016) Carboxymethyl chitosan-modified magnetic-cored dendrimer as an amphoteric adsorbent. *J Hazard Mater* 317:608–616
- [36] Pilapong C, Raiputta C, Chaisupa J, Sittichai S, Thongtem S, Thongtem T (2015) Magnetic-EpCAM nanoprobe as a new platform for efficient targeting, isolating and imaging hepatocellular carcinoma. *RSC Adv* 5(39):30687–30693
- [37] Griffete N, Herbst F, Pinson J, Ammar S, Mangeney C (2011) Preparation of water-soluble magnetic nanocrystals using aryl diazonium salt chemistry. *J Am Chem Soc* 133(6):1646–1649
- [38] Osaka T, Matsunaga T, Nakanishi T, Arakaki A, Niwa D, Iida H (2006) Synthesis of magnetic nanoparticles and their application to bioassays. *Anal Bioanal Chem* 384(3):593–600
- [39] Larrubia MA, Ramis G, Busca G (2000) An FT-IR study of the adsorption of urea and ammonia over V₂O₅-MoO₃-TiO₂ SCR catalysts. *Appl Catal B* 27(3):L145–L151
- [40] Ma M, Zhang Y, Yu W, H-y Shen, Zhang H-q GuN (2003) Preparation and characterization of magnetite nanoparticles coated by amino silane. *Colloids Surf A* 212(2–3):219–226
- [41] Cao H, He J, Deng L, Gao X (2009) Fabrication of cyclodextrin-functionalized superparamagnetic Fe₃O₄/amino-silane core-shell nanoparticles via layer-by-layer method. *Appl Surf Sci* 255(18):7974–7980
- [42] Čampelj S, Makovec D, Drogenik M (2009) Functionalization of magnetic nanoparticles with 3-aminopropyl silane. *J Magn Magn Mater* 321(10):1346–1350

- [43] Lei Z, Li Y, Wei X (2008) A facile two-step modifying process for preparation of poly(SStNa)-grafted $\text{Fe}_3\text{O}_4/\text{SiO}_2$ particles. *J Solid State Chem* 181(3):480–486
- [44] Wang L, Duan G, Chen S-M, Liu X (2015) Particle size and dispersity control by means of gelatin for high-yield mesoporous silica nanospheres. *Ind Eng Chem Res* 54(50):12580–12586
- [45] Popovic J, Hasegawa G, Moudrakovski I, Maier J (2016) Infiltrated porous oxide monoliths as high lithium transference number electrolytes. *J Mater Chem A* 4(19):7135–7140
- [46] Ko J, Lee J, Yoo B, Ryu J, Sohn D (2016) Capillarity-induced selective ex situ synthesis of metal–organic framework inside mesoporous nanotubes. *Microporous Mesoporous Mater* 220:16–20
- [47] Wang S, Wang K, Dai C, Shi H, Li J (2015) Adsorption of Pb^{2+} on amino-functionalized core–shell magnetic mesoporous SBA-15 silica composite. *Chem Eng J* 262:897–903
- [48] Ahmed MA, Ali SM, El-Dek SI, Galal A (2013) Magnetite–hematite nanoparticles prepared by green methods for heavy metal ions removal from water. *Mater Sci Eng B* 178(10):744–751
- [49] Yu J-X, Wang L-Y, Chi R-A, Zhang Y-F, Xu Z-G, Guo J (2013) Competitive adsorption of Pb^{2+} and Cd^{2+} on magnetic modified sugarcane bagasse prepared by two simple steps. *Appl Surf Sci* 268:163–170
- [50] Gan T, Wu K (2008) Sorption of $\text{Pb}(\text{II})$ using hydrogen peroxide functionalized activated carbon. *Colloids Surf A* 330(2–3):91–95
- [51] Zhang F, Wang B, He S, Man R (2014) Preparation of graphene-oxide/polyamidoamine dendrimers and their adsorption properties toward some heavy metal ions. *J Chem Eng Data* 59(5):1719–1726
- [52] Bai L, Hu H, Fu W, Wan J, Cheng X, Zhuge L et al (2011) Synthesis of a novel silica-supported dithiocarbamate adsorbent and its properties for the removal of heavy metal ions. *J Hazard Mater* 195:261–275
- [53] Taty-Costodes VC, Fauduet H, Porte C, Delacroix A (2003) Removal of $\text{Cd}(\text{II})$ and $\text{Pb}(\text{II})$ ions, from aqueous solutions, by adsorption onto sawdust of *Pinus sylvestris*. *J Hazard Mater* 105(1–3):121–142
- [54] Orolínoová Z, Mockovčiaková A, Škvarla J (2012) Sorption of cadmium (II) from aqueous solution by magnetic clay composite. *Desalination Water Treat* 24(1–3):284–292
- [55] Alsohaimi IH, Wabaidur SM, Kumar M, Khan MA, Allothman ZA, Abdalla MA (2015) Synthesis, characterization of PMDA/TMSPEDA hybrid nano-composite and its applications as an adsorbent for the removal of bivalent heavy metals ions. *Chem Eng J* 270:9–21
- [56] Azouaou N, Sadaoui Z, Djaafri A, Mokaddem H (2010) Adsorption of cadmium from aqueous solution onto untreated coffee grounds: equilibrium, kinetics and thermodynamics. *J Hazard Mater* 184(1–3):126–134
- [57] Foo KY, Hameed BH (2010) Insights into the modeling of adsorption isotherm systems. *Chem Eng J* 156(1):2–10
- [58] Yakout AA, El-Sokkary RH, Shreadah MA, Abdel Hamid OG (2016) Removal of $\text{Cd}(\text{II})$ and $\text{Pb}(\text{II})$ from wastewater by using triethylenetetramine functionalized grafted cellulose acetate-manganese dioxide composite. *Carbohydr Polym* 148:406–414
- [59] Benhima H, Chiban M, Sinan F, Seta P, Persin M (2008) Removal of lead and cadmium ions from aqueous solution by adsorption onto micro-particles of dry plants. *Colloids Surf B Biointerfaces* 61(1):10–16
- [60] Zhu C, Liu F, Xu C, Gao J, Chen D, Li A (2015) Enhanced removal of $\text{Cu}(\text{II})$ and $\text{Ni}(\text{II})$ from saline solution by novel dual-primary-amine chelating resin based on anion-synergism. *J Hazard Mater* 287C:234–242
- [61] Park JH, Ok YS, Kim SH, Cho JS, Heo JS, Delaune RD et al (2016) Competitive adsorption of heavy metals onto sesame straw biochar in aqueous solutions. *Chemosphere* 142:77–83
- [62] Prasher SO, Beauguard M, Hawari J, Bera P, Patel RM, Kim SH (2004) Biosorption of heavy metals by red algae (*Palmaria palmata*). *Environ Technol* 25(10):1097–1106
- [63] Misono M, Ei Ochiai, Saito Y, Yoneda Y (1967) A new dual parameter scale for the strength of Lewis acids and bases with the evaluation of their softness. *J Inorg Nucl Chem* 29(11):2685–2691